

Development of rate-dependent constitutive model for elastomers

A.F.M.S.Amin, M.S.Alam & Y.Okui

Department of Civil and Environmental Engineering, Saitama University, Japan

00303

ABSTRACT: Equilibrium and instantaneous elastic responses from a solid enclose the boundary of the viscous domain where rate-dependent effect comes into play. However, due to experimental limitation, direct application of infinite slow or fast motions on the material is not practical to get such responses for determining material parameters. To this end, an experimental scheme for elastomeric materials has been proposed to identify the elastic parameters through extrapolation and using hyperelasticity model. In this course, an approach for developing finite deformation rate-dependent model incorporating modified hyperelasticity function has been introduced. The aspects of determining the viscosity parameter using the finite deformation model have been discussed. The adequacy of the proposed viscoelasticity parameter determination procedure in simulating the experimental results has been verified using the numerical model.

1 INTRODUCTION

Traditionally elastomeric materials find wide engineering applications in structural components like bridge bearings, shock absorbers etc. Recently, lead plugged natural rubber bearings (commonly known as lead rubber bearing) have been used in base isolation systems of earthquake resistant structures. Furthermore, for such specific end use, new special elastomers like high damping rubbers (HDR) with better energy absorption property have been developed. Unlike other elastomeric materials, HDR exhibits a rate-dependent elastic response. However, when subjected to cyclic loading, significant amount of hysteresis and permanent set also occur. Because of such features, the constitutive behavior of this material is not yet fully understood. Hence there exists the necessity to develop a rational constitutive model for simulating the mechanical response of HDR for using in analysis and design computations.

Generally, hyperelasticity laws are used to model the elastomeric response under monotonic loading. However, such approach can not model the rate-dependent behavior. So for developing a rate-dependent constitutive model for this range of materials, a rate-dependent hyperelasticity modeling is needed. Hence, the objective of this paper is to present an approach for developing a model to simulate the nonlinear rate-dependent behavior of the material. This paves the way for developing a complete model which will be able to simulate the cyclic response as well.

Figure 1 presents schematic representation of the viscoelastic domain. In a typical viscoelastic solid loaded in an infinitely slow rate, the stress-strain curve follows the E-E' path giving the equilibrium response. On the other hand, in case of infinitely fast motion, the response takes the I-I' path. Such response is known as instantaneous response. Both equilibrium and instantaneous response are elastic response and the domain of viscosity lies in between these two states (Huber & Tsakmakis 2000). Thus, elastic parameters determine the boundary of the domain where viscosity comes into play. These parameters need to be determined from experimental data.

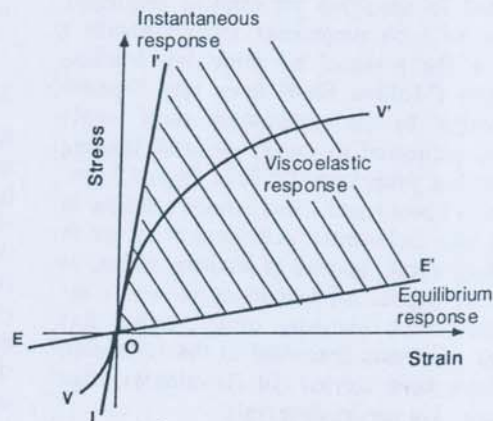


Figure 1. Typical responses from a viscoelastic solid.

However, from a practical point of view, neither infinite slow motion nor infinite fast motion is possible due to experimental limitation. In this situation, parameter determination process solely depends on numerical trials, which is not meaningful from physical point of view.

The paper presents an experimental scheme to identify the material parameters for equilibrium and instantaneous responses. In this course a finite deformation viscoelasticity model has been employed and parameter estimation process has been discussed. Finally numerical simulation results obtained from the model have been presented to discuss the adequacy of the proposed procedure.

2 EXPERIMENTAL OBSERVATION

An experimental scheme comprising of a multi-step relaxation test, monotonic compression tests and simple relaxation tests has been carried out to identify elasticity and viscosity parameters. All tests were carried out on pre-loaded specimens. The following subsections present the details of the experiments and salient features observed therein.

2.1 Experimental setup

In the present study, cubic specimens (50mm x 50mm x 50mm) were tested in a computer-controlled servohydraulic testing machine. In order to cut friction between the sample and the loading plates, polypropylene films with lubricant on top and bottom of the sample were used. The axial force and the displacement were recorded using a personal computer. The applied stretch (i.e. $1+dL/L$, where L is the undeformed length) and the Cauchy stress (true stress) were calculated under the assumptions of homogenous deformation and incompressibility of the specimens, respectively.

2.2 Pre-loading

Prior to the actual experiment, all virgin specimens were subjected to specified pre-loading sequence. The objective of such preprocess was to obtain a stable state in the material by removing Mullins softening effect (Mullins 1969) from rate dependency phenomena. In the pre-process each virgin specimen was subjected to cyclic uniaxial loading for 5 cycles with a strain rate of 0.01/s. Figure 2 presents the stretch history and stress-stretch relation in a pre-loading test. Substantial softening behavior in the first loading cycle, known as Mullins effect, is evident from the figure. All specimens showed a repeatable stress-stretch response after passing 2-3 loading cycles. All tests described in the following subsections have been carried out 20 minutes after the end of respective pre-loading tests.

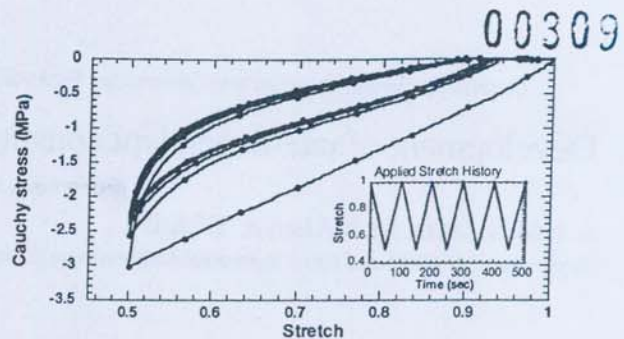


Figure 2. Applied stretch history and stretch-stress response observed in pre-loading.

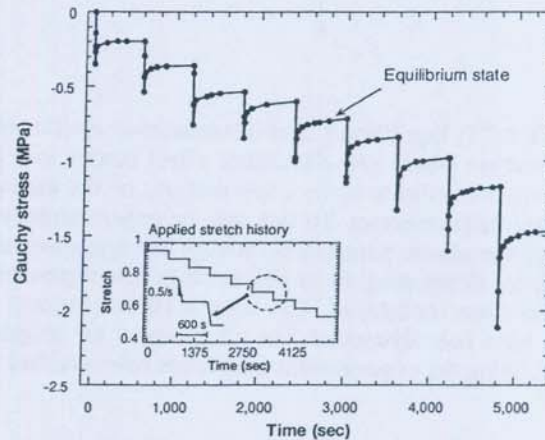


Figure 3. Applied stretch history and stretch-stress response observed in multi-step relaxation test.

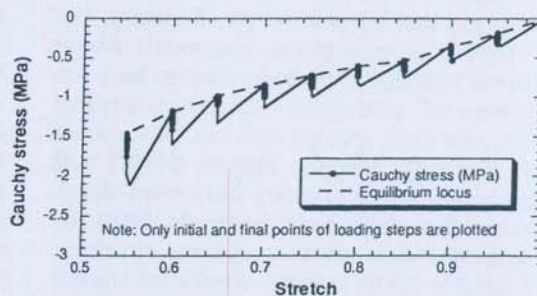


Figure 4. Stretch-stress response and approximated equilibrium locus obtained from multi-step relaxation test.

2.3 Multi-step relaxation test

Ideally, the equilibrium response is obtained when a material is loaded at infinitely slow rate. However, in case of highly viscous materials like elastomers it is quite difficult to specify a slow loading rate where the viscosity effect can be ruled out. In the current study, a multi-step relaxation test has been carried out to identify the equilibrium locus over the considered stretch range. Figure 3 presents the applied stretch and obtained stress history of the test. It is seen that, at the end of each relaxation interval of 10

min. duration, the stress relaxes to an apparent equilibrium state. Although such an equilibrium state can only be achieved in an asymptotic sense, these stages invariably indicate the neighborhood of equilibrium state. Figure 4 presents the stretch-stress response together with the approximated equilibrium locus in a multi-step relaxation test.

2.4 Monotonic compression test

The instantaneous elastic response of a solid is ideally obtained when the material is loaded at infinite fast rate. From an experimental point of view, however, there is a finite maximum value of stroke rate for any displacement controlled loading device. Although the loading rate on a specimen can be increased by using a smaller specimen dimension in the loading direction, the reduced aspect ratio of the specimen increases the boundary effects on other turn. In this context to find a method for estimating the instantaneous response of the material, a series of monotonic compression tests each at different but constant strain rate has been carried out. In the test sequence, strain rates were varied from 0.001/s to 0.96/s. For simplicity in illustration, Figure 5 shows the rate-dependent stress-strain responses observed only for the cases at strain rates of 0.001/s, 0.025/s, 0.075/s, 0.225/s, 0.47/s and 0.96/s respectively. The equilibrium locus as obtained from Figure 4 has also been compared here with the cases of different strain rates. The comparison of the curves displays the increase of stress response with increasing applied strain rate due to rate-dependency phenomena. However, at higher strain rates a diminishing trend in the increase of stress response is observed. From these data, the instantaneous response will be extrapolated which will be shown in the next section.

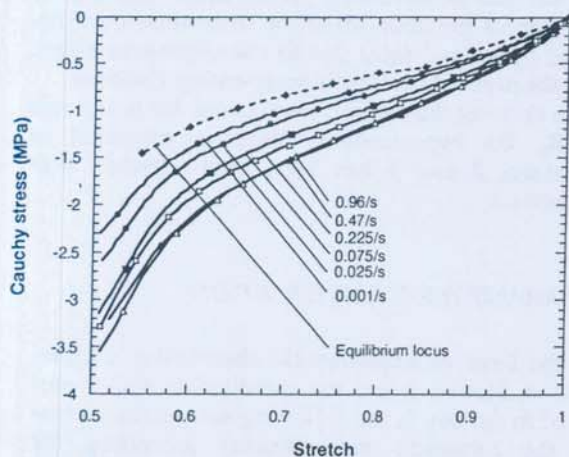


Figure 5. Comparison of monotonic compression test stretch-stress responses at different strain rates along with the equilibrium locus.

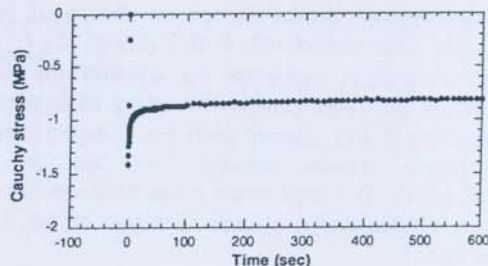


Figure 6. Stress history obtained from simple relaxation test at 0.7 stretch level.

2.5 Simple relaxation test

In order to observe the viscosity induced stress-relaxation phenomena, simple relaxation tests have been carried out at different stretch levels. Similar to the multi-step relaxation test, the strain rate in the loading phase was maintained at 0.5/s followed by a hold time of 10 min. in each test. Figure 6 presents the stress history obtained from the test at 0.7 stretch level. The figure illustrates a rapid stress relaxation feature of the material in the first 2 min. of hold time after which it approaches asymptotically towards an equilibrium state.

3 CONSTITUTIVE MODEL

The experimental observation summarized in Section 2 revealed the strain rate dependency of the material. Typically hyperelasticity laws can be used for modeling elastomeric response for a particular strain rate. However, for modeling nonlinear strain rate dependency of the material, hyperelasticity laws need to be combined with a rate-dependent model. The following subsections summarize the aspects of model configuration, the approaches for hyperelasticity, and rate-dependency modeling.

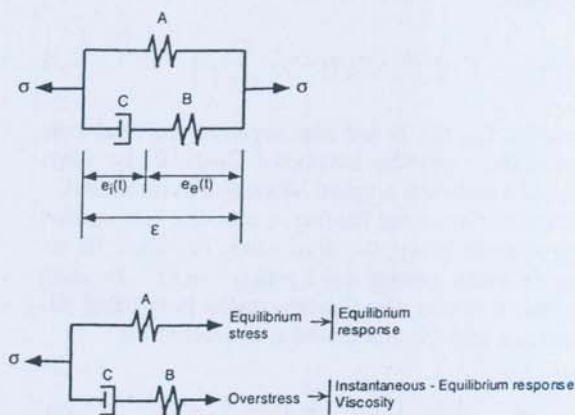


Figure 7. Three-parameter parallel model.

3.1 Model configuration

A three-parameter parallel model as illustrated in Figure 7 has been considered. In this model, the hyperelastic element A represents the equilibrium response, while the other branch consisting of hyperelastic element B and viscous dash-pot C represents the over-stress feature coming from the rate-dependent effect. The total strain ϵ has been decomposed into elastic strain e_e and inelastic strain e_i components.

3.2 Hyperelasticity modeling

In a phenomenological approach, under the assumption of isotropy, elastomeric materials are represented in terms of a strain energy density function W . Such functions for elastomers are expressed either in terms of the strain invariants or principal stretches. The strain-invariant-based models are easy to implement in a mathematical formulation, while the stretch based models suggest to be more flexible in fitting experimental data particularly at higher strain levels. However to follow a simpler computational approach, this paper chooses strain-invariant-based hyperelasticity models. In this approach, the three strain invariants (i.e. I, II, III) are expressed as:

$$\begin{aligned} I &= \text{tr} \mathbf{B} = \lambda_1^2 + \lambda_2^2 + \lambda_3^2 \\ II &= \text{tr} \mathbf{B} \mathbf{B} = (\lambda_1 \lambda_2)^2 + (\lambda_2 \lambda_3)^2 + (\lambda_3 \lambda_1)^2 \\ III &= \det \mathbf{B} = (\lambda_1 \lambda_2 \lambda_3)^2 \end{aligned} \quad (1)$$

where $\lambda_1, \lambda_2, \lambda_3$ are the principal stretches; left Cauchy-Green deformation tensor, $\mathbf{B} = \mathbf{F} \mathbf{F}^T$; \mathbf{F} = deformation gradient tensor.

Among the strain invariant based models, Mooney-Rivlin model is the most common one but does not perform well at higher strain levels. To solve this problem, a higher order function of I as proposed by Yamashita & Kawabata (1992) has been incorporated in this study for modeling the responses at higher strain levels. Equation 2 presents the strain energy density function of the hyperelasticity model.

$$W(I, II) = C_5(I-3) + C_2(II-3) + \frac{C_3}{N+1}(I-3)^{N+1} \quad (2)$$

where C_5, C_2, C_3, N are non-negative material constants. Here with the parameter $C_3=N=0$ the functions reduces to the original Mooney-Rivlin model.

In case of uniaxial loading, under the assumption of incompressibility, the third strain invariant III reduces to unity giving $\lambda_2 = \lambda_3 = (\lambda_1)^{-\frac{2}{3}} = (\lambda)^{-\frac{2}{3}}$. In such case, the function for Cauchy stress in loading direction (i.e. σ_1) for this model is expressed as:

$$\sigma_1 = 2(\lambda^2 - \frac{1}{\lambda}) [C_5 + \frac{1}{\lambda} C_2 + C_3(\lambda^2 + \frac{2}{\lambda} - 3)^N] \quad (3)$$

In the stretch-stress relation, C_5 component dominates over the entire stretch regime of both tension and compression. However, the effect of C_2 component is effective only at tension zone (particularly at low stretch levels) in representing the characteristic 'S' shape stress-stretch relation. In contrast to these, the effect of C_3 component with an exponential term N is effective only at higher stretch levels.

3.3 Rate-dependency modeling

The stress and strain components of the three-parameter parallel model presented in Figure 7 has been converted into its finite deformation counterparts following the formulation of Huber & Tsakmakis (2000). The finite deformation model has been formulated under the framework of multiplicative decomposition of \mathbf{F} . Here the equilibrium strains e_e and e_i (Fig. 7) are related to equilibrium and intermediate equilibrium parts \mathbf{F}_e and \mathbf{F}_i so that $\mathbf{F} = \mathbf{F}_e \mathbf{F}_i$. This leads the Cauchy stress tensor \mathbf{S} and rate of left Cauchy-Green deformation tensor \mathbf{B} as follows:

$$\mathbf{S} = -p\mathbf{I} + \mathbf{S}_E \quad (4a)$$

$$\mathbf{S}_E = \mathbf{S}_E^{(E)} + 2 \frac{\partial W'}{\partial \mathbf{I}_{B_e}} \mathbf{B}_e - 2 \frac{\partial W'}{\partial \Pi_{B_e}} \mathbf{B}_e^{-1} \quad (4b)$$

$$\mathbf{S}_E^{(E)} = 2 \frac{\partial W^{(E)}}{\partial \mathbf{I}_B} \mathbf{B} - 2 \frac{\partial W^{(E)}}{\partial \Pi_B} \mathbf{B}^{-1} \quad (4c)$$

$$\dot{\mathbf{B}}_e = \mathbf{B}_e \mathbf{L}^T + \mathbf{L} \mathbf{B}_e - \frac{2}{\eta} \mathbf{B}_e (\mathbf{S}_E - \mathbf{S}_E^{(E)})^D \quad (4d)$$

where p is the hydrostatic pressure of \mathbf{S} and subscript 'E' denotes the extra part of corresponding stress tensor. \mathbf{I} is the identity matrix. The super-script '(E)' denotes the equilibrium stress while the subscript 'e' denotes equilibrium part of the strain tensor. \mathbf{L} is the velocity gradient tensor. Super-script 'D' denotes the deviatoric part of stress. The derivative part of Equation 4b is the over-stress part (denoted by 'prime' sign) due to rate-dependent effect. η is the material parameter representing viscosity.

In deriving the explicit expressions for \mathbf{S} and rate of \mathbf{B}_e , the hyperelasticity function presented in Equations 2 and 3 has been used together with Equation 4.

4 PARAMETER IDENTIFICATION

On the basis of experimental observation summarized in Section 2 and the constitutive model presented in Section 3, the following sub-sections present the parameter determination procedure for representing equilibrium response, instantaneous response, and viscosity effect.

4.1 Equilibrium response

The hyperelasticity model coefficients for the equilibrium locus obtained from the multi-step relaxation tests (Sec. 2.3) have been determined by a best-fit technique. Since the experimental observation was carried out in compression regime, there is no effect of C_2 coefficient for this zone. Hence to avoid getting negative values in curve fitting, C_2 was assigned to zero. The values of the parameters are listed in Table 1.

Table 1. Elastic material parameters

State	C_5 MJm ⁻²	C_3 MJm ⁻²	C_2 MJm ⁻²	N MJm ⁻²
Equilibrium	0.48	0.015	0.00	3.30
Instantaneous	0.85	0.120	0.00	3.30

4.2 Instantaneous response

The monotonic compression tests presented in Section 2.4 displayed a diminishing trend in an increase of the stress-strain response at higher strain rates indicating the approach of the instantaneous state. Interestingly, the overall stress-stretch response at each strain rate has a characteristic 'S' shaped curve, which can be described by the coefficients of the hyperelasticity model. On the basis of this feature, the hyperelasticity constants i.e. C_5 and C_3 have been determined for a constant value of N (as determined from the equilibrium locus) for different strain rate cases over the range of 0.001/s - 0.96/s. The C_5 and C_3 parameters determined this way have been plotted respectively in Figures 8 and 9 against the corresponding strain rate values.

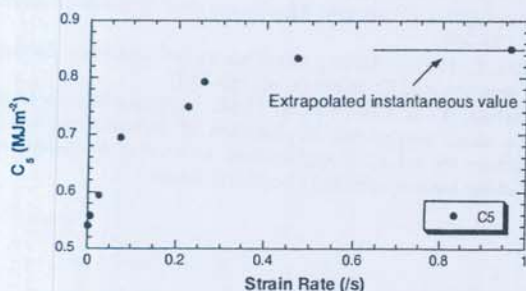


Figure 8. C_5 parameter as a function of strain rate.

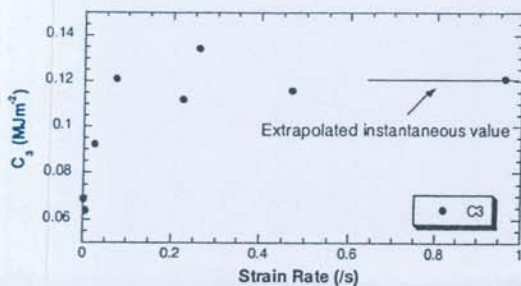


Figure 9. C_3 parameter as a function of strain rate.

It is interesting to note that the values of C_5 and C_3 parameters (Figs. 8,9) reach an asymptotic path over the strain rate of 0.25/s. This must be due to approach of the instantaneous state. The parameters for the instantaneous response are estimated from this asymptotic trend within finite strain rate region. The values of the parameters have been presented in Table 1. The subtraction of the values of C_5 , C_3 , C_2 from the instantaneous to equilibrium state gives the parameter values for the overstress response.

4.3 Viscosity

After determining the elastic parameters for the instantaneous and equilibrium response, the only remaining unknown is the viscosity parameter η representing dash-pot viscosity (Fig. 7). Here, simple relaxation test data has been used to obtain η through simulation trials of the rate-dependent hyperelasticity model (Sec. 3.3) by comparing the computed stress relaxation rate with experimental data.

For the relaxation test at 0.7 stretch level, $\eta = 1.125$ MPas represented the relaxation feature adequately (Figure 10). The parameter determined this way has been confirmed with simple relaxation data at other stretch levels.

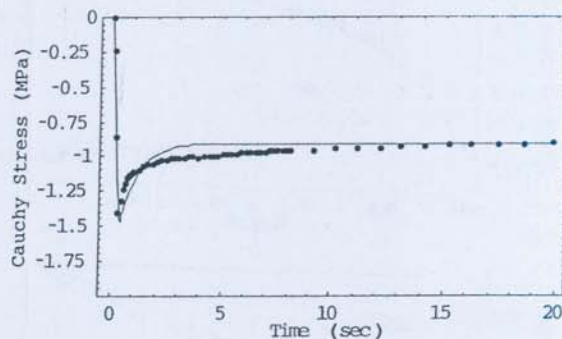


Figure 10. Optimization of viscosity parameter by simulating the simple relaxation test result (-) Numerical simulation, (●) Experiment

5 NUMERICAL SIMULATION

Using the parameters determined in the preceding section, the model has been used to simulate the monotonic compression test at varied strain rates. Figure 11 presents the simulation results in comparison with experimental data, where a good conformity is observed. However, as expected, the representation of stress-stretch response at low stretch levels is a bit poor particularly at lower strain rates due to the limitation of hyperelastic model in that region. As a general trend, the numerical results slightly under estimated the response in all strain rate cases.

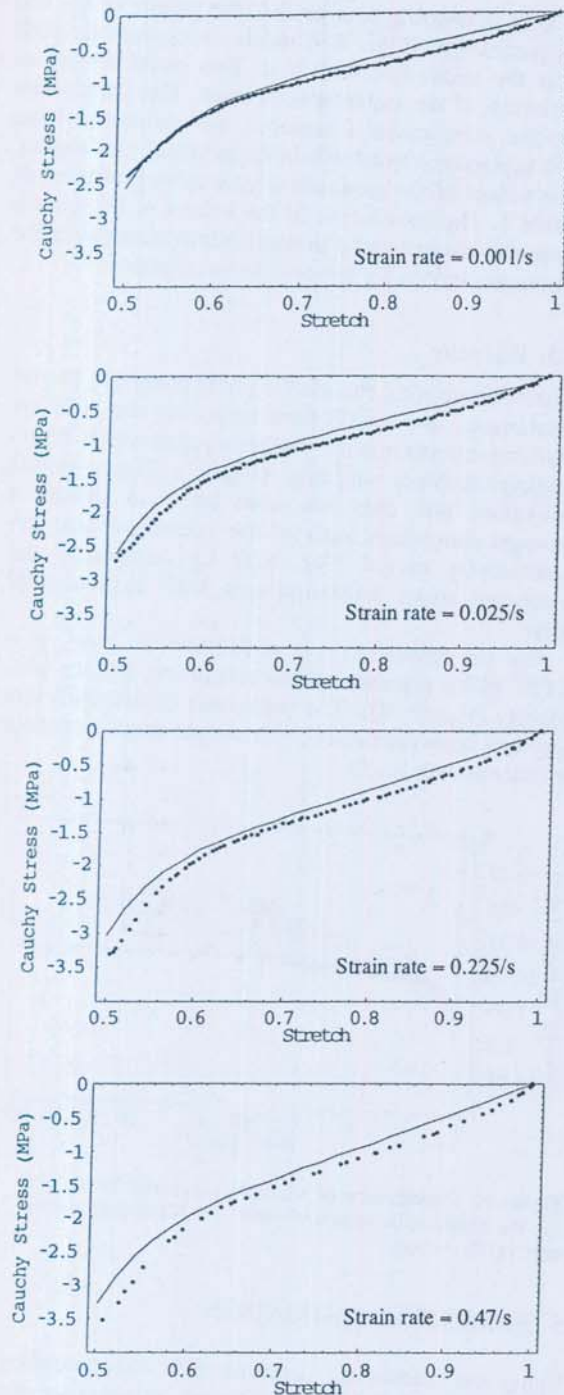


Figure 11. Numerical simulation of monotonic compression test at different strain rates. (-) Numerical simulation, (•) Experiment

6 CONCLUSIONS

The locus of equilibrium response of elastomers can be approximated from a multi-step relaxation experiment. However, for estimating instantaneous response, a series of monotonic uniaxial compression

tests with increasing strain rate is needed. The hyperelasticity model can then be used to find the parameters for equilibrium and instantaneous responses from these experimental data. In this connection, incorporation of an exponential term as proposed by Yamashita & Kawabata (1992) in the strain energy density formulation has been found to improve the stress-stretch representation at higher stretch level. After identifying the elastic parameters, the rate-dependent finite deformation hyperelasticity model can be used to find the viscosity parameter by comparing the simple relaxation test data. The comparison of numerical results with monotonic compression test results at varied strain rates has showed the adequacy of the proposed procedure. Although the parameter identification procedure and constitutive model presented in the paper are discussed in compression regime only, these are applicable for tension regime as well.

ACKNOWLEDGEMENT

The authors express their deep sense of gratitude to Professor H. Horii, Department of Civil Engineering, Tokyo University, Japan for extending experimental facility of his laboratory to carry out the experimental part of the work described in the paper.

REFERENCES

- Huber, N. & Tsakmakis, C. 2000. Finite deformation viscoelasticity laws. *Mechanics of Materials*. 32:1-18.
- Lion, A. 1996. A constitutive model for carbon black filled rubber: Experimental investigations and mathematical representation. *Continuum Mechanics and Thermodynamics*. 8:153-169.
- Mullins, L. 1969. Softening of rubber by deformations. *Rubber Chemistry and Technology*. 42:339-362.
- Yamashita, Y. & Kawabata, S. 1992. Approximated form of the strain energy density function of carbon-black filled rubbers for industrial applications. *Journal of the Society of Rubber Industry*. 65(9):517-528. (in Japanese)